

Hints of dark energy anisotropic stress using Machine Learning

Rubén Arjona* and Savvas Nesseris†

Instituto de Física Teórica UAM-CSIC, Universidad Autónoma de Madrid, Cantoblanco, 28049 Madrid, Spain

(Dated: June 17, 2022)

Recent analyses of the Planck data and quasars at high redshifts have suggested possible deviations from the flat Λ cold dark matter model (Λ CDM), where Λ is the cosmological constant. Here, we use machine learning methods to investigate any possible deviations from Λ CDM at both low and high redshifts by using the latest cosmological data. Specifically, we apply the genetic algorithms to explore the nature of dark energy (DE) in a model independent fashion by reconstructing its equation of state $w(z)$, the growth index of matter density perturbations $\gamma(z)$, the linear DE anisotropic stress $\eta_{DE}(z)$ and the adiabatic sound speed $c_{s,DE}^2(z)$ of DE perturbations. We find a $\sim 2\sigma$ deviation of $w(z)$ from -1 at high redshifts, the adiabatic sound speed is negative at the $\sim 2\sigma$ level and a $\sim 3\sigma$ deviation of the anisotropic stress from unity at low redshifts and $\sim 3.5\sigma$ at high redshifts. These results suggest either the presence of a strong non-adiabatic component in the DE sound speed or the presence of DE anisotropic stress, thus hinting at possible deviations from the Λ CDM model.

I. INTRODUCTION

Through the observations of distant Type Ia supernovae at the turn of the previous century, it was discovered that the Universe is undergoing a phase of accelerated expansion on very large scales, apparently caused by a repulsive force, usually attributed to the cosmological constant [1, 2]. Further observations and theoretical developments led to a unified description for the formation and evolution of the Universe within the framework of General Relativity (GR), known as the standard Λ cold dark matter model (Λ CDM), that contains only six free parameters describing the matter and dark energy (DE) content of the Universe. This model is so far the best phenomenological fit to the data [3].

While this framework is very successful, there also remain some tensions to resolve, such as the nature of the dominant cold dark matter component or the hotly debated Hubble constant tension, where the determination of H_0 deduced from physics of the early universe, i.e. the cosmic-microwave-background (CMB) observations [3], is lower than the local determination of H_0 based on Cepheid variable-calibrated Type Ia supernovae (SNIa) [4] at the 4.4σ confidence level. Also, as mentioned in Ref. [5], results from other collaborations such as DES [6], SPT Collaboration [7] or the H0LiCOW collaboration [8], with no common observational systematics between them, add to the idea that the tension is due more to the physics of the cosmological setting rather than experimental systematics, see Refs. [9, 10] and references therein for a recent discussion.

However, recently other tensions have also appeared. Using quasars in high redshifts up to $z \simeq 7.5$, it was shown in Ref. [11] that a $\sim 4\sigma$ deviation from the Λ CDM model exists, suggesting a time evolution of the DE equation of state at high redshifts. On the other hand, in

Ref. [12] it was shown that an enhanced lensing amplitude still present in the Planck 2018 CMB data, can be explained by a positive curvature Universe, thus violating the underlying assumptions of the flat Λ CDM model.

These issues have motivated several analyses trying to reassess the level of tensions and deviations from the Λ CDM model [13–19] or to resolve it with new physics [20]. The latter approach postulates that GR is only accurate on small scales and modifications at larger scales are needed. One side-effect of this deviation from GR is that the Newtonian potentials Φ and Ψ are now in general not equal, thus resulting to an anisotropic stress which could be detected from weak-lensing [21]. The anisotropic stress is usually modeled via the parameter $\eta_{DE} \equiv \frac{\Phi}{\Psi}$, where Φ and Ψ are the Newtonian potentials, taken to be equal in GR in the absence of anisotropic stresses from other sources such as neutrinos. Thus, any deviation of η_{DE} from unity would point to modified gravity or if neglected, it could bias the cosmological parameters inferred from the data [22].

If this modification of gravity is interpreted via the effective fluid approach [23, 24], then the presence of anisotropic stress also implies the sound speed of propagation of the DE perturbations $c_{s,DE}^2$ can be negative. However, the perturbations can still remain stable if the effective sound speed, defined as the sum of the DE sound speed and the anisotropic stress, is positive [25]. Therefore, if direct measurements of $c_{s,DE}^2$ find that it is negative, this would be a smoking gun signature for the existence of an anisotropic stress and possible modifications of gravity. Furthermore, it has been shown that the effects of the anisotropic stress can be mimicked by a varying adiabatic sound speed of DE perturbations [26, 27]. A related quantity is also the $F(z)$ test of Ref. [28], which is proportional to the DE sound speed and is supposed to be equal to zero for the Λ CDM model. As both $F(z)$ and $c_{s,DE}^2$ are related, here we will only consider the latter.

The large scale structure (LSS) of the Universe provides a natural testbed for searching for deviations from GR, since it is very sensitive to the underlying gravitational theory which directly affects the evolution of mat-

*Electronic address: ruben.arjona@uam.es

†Electronic address: savvas.nesseris@csic.es

ter density perturbations. In linear theory these are parameterized via the growth parameter $\delta_m = \frac{\delta \rho_m}{\bar{\rho}_m}$ and its logarithmic derivative $f \equiv \frac{d \ln \delta_m}{d \ln a}$ called the growth-rate, where $\bar{\rho}_m$ is the background matter density and $\delta \rho_m$ its perturbation to linear order. The growth-rate can also be expressed in terms of the γ parameter, which is useful when looking for deviations from GR, as in the Λ CDM model $\gamma \simeq 6/11$ and is defined via $f(z) = \Omega_m^\gamma(z)$. In the Λ CDM model, the fact that the growth rate is scale-invariant on large scales makes it a key discriminator [29].

The main advantage of the growth is that over time it can provide information about gravity and DE and how both can be evolving as the Universe expands. The reason for this is that LSS observations in cosmology have the advantage of requiring only linear physics, which makes them an especially clean and highly successful probe [30]. They can help in the understanding what is the expansion rate of the Universe and how do structures form within the cosmological background.

At the perturbations level, the growth of matter perturbations provides a useful tool to investigate the matter distribution in the Universe, and, more importantly, it can be measured from observations. The measurement of the growth index provides an efficient way to discriminate between modified gravity models and DE models which are developed in the context of GR [31]. The effect of DE on the growth of perturbations is therefore an important tool in discriminating models from Λ CDM [32] and models that are fully degenerate at the background level [23, 33–36].

Cosmology has now reached a level of precision allowing it to become a complementary probe of particle and fundamental physics. Observations of future experiments such as LSST [37], DES [38], eBOSS [39], J-PAS [40], DESI [41], SKA [42] and 21-cm data [43] will allow us to probe the whole epoch from recombination to now and provide a vast amount of data for a broad span of redshifts with hundreds of thousands of supernovas type Ia, along with millions of galaxies and quasars.

Clearly, the acquisition of such vast amounts of data means that traditional statistical inference is impractical, as the dimensionality of the data will also increase exponentially, a phenomenon known as “curse of dimensionality” [44]. This makes it an excellent testing ground for machine learning (ML) methods as the latter are ideal in cases where traditional fitting methods give poor results or completely fail, such as in the case of big data, but also when the parameter space is very large, too complex or not well enough understood, as is the case of DE.

Machine learning will play a big role in testing accurately the standard model of cosmology, but will also help in the search for new physics and tensions in the data by placing tighter constraints on cosmological parameters [45]. While a central goal of modern ML research is to learn and extract important features directly from data [46], ML methods have also been applied to reconstruct null tests of Λ CDM, i.e. quantities that are supposed to be exactly constant for all redshifts [47–53].

In this paper we present a unified ML analysis of all the currently available cosmological data in order to reconstruct several key background and perturbations variables in a model-independent manner in order to explore the nature of DE. For example, such variables include the DE equation of state and the DE anisotropic stress, which we then use to test for deviations from Λ CDM.

The structure of our paper is as follows: In Section II we present our methodology and the minimal assumptions we made for the reconstruction of the data. In Section III we present our main results, while in Section IV we present our Conclusions. Finally, in Appendix A we describe in detail the data we used in our analysis, in Appendix B we present some more theoretical details about various theoretical quantities and our notation, in Appendix C we present the exact fits of the reconstruction and in Appendix D we describe our error analysis.

II. ANALYSIS

We will now describe how to reconstruct the Hubble parameter $H(z)$ from the Hubble expansion history $H(z)$ data, the luminosity distance $d_L(z)$ from the Pantheon Type Ia supernovae (SnIa) data, the angular diameter distance $d_A(z)$ from Baryon Acoustic Oscillations (BAO), $f\sigma_8(z)$ from the growth-rate data obtained via the redshift-space distortions (RSD) and $P_2(z)$ from the E_g data. All of the aforementioned quantities are described in detail in Appendix A.

These functions will in turn be used to reconstruct the DE anisotropic stress $\eta_{DE}(z)$, the growth index $\gamma(z)$, the DE equation of state $w(z)$ and the DE adiabatic sound speed $c_{s,DE}^2(z)$. Furthermore, we will also reconstruct the growth rate null test $\mathcal{O}(z)$ presented in Ref. [54] as a consistency test of the Λ CDM model and the number counts of luminous sources $n(z)$. We also derive the matter density $\Omega_{m,0}$ and the root mean square (rms) density fluctuation σ_8 from the $f\sigma_8$ data, the value of the Hubble constant H_0 and the sound horizon at the drag epoch r_d from the BAO data.

The reconstruction method we use is a particular ML approach known as Genetic Algorithms (GA). The GA represents a method for non-parametric reconstruction of functions, based on the notions of grammatical evolution and the genetic operations of mutation and crossover, which are applied probabilistically to a population of functions created by a grammar during every generation. The main advantage of the GA is that it requires very minimal a priori assumptions about the underlying data and more importantly in our case, it requires no assumptions of a DE model or a spatially flat Universe.

Furthermore, it has been shown that the choice of the grammar only affects the rate of convergence [55]. For more details on the GA and various applications to cosmology see [55],[56]. On the other hand, other non-parametric approaches such as the gaussian processes (GP) require the choice of a kernel function and that of

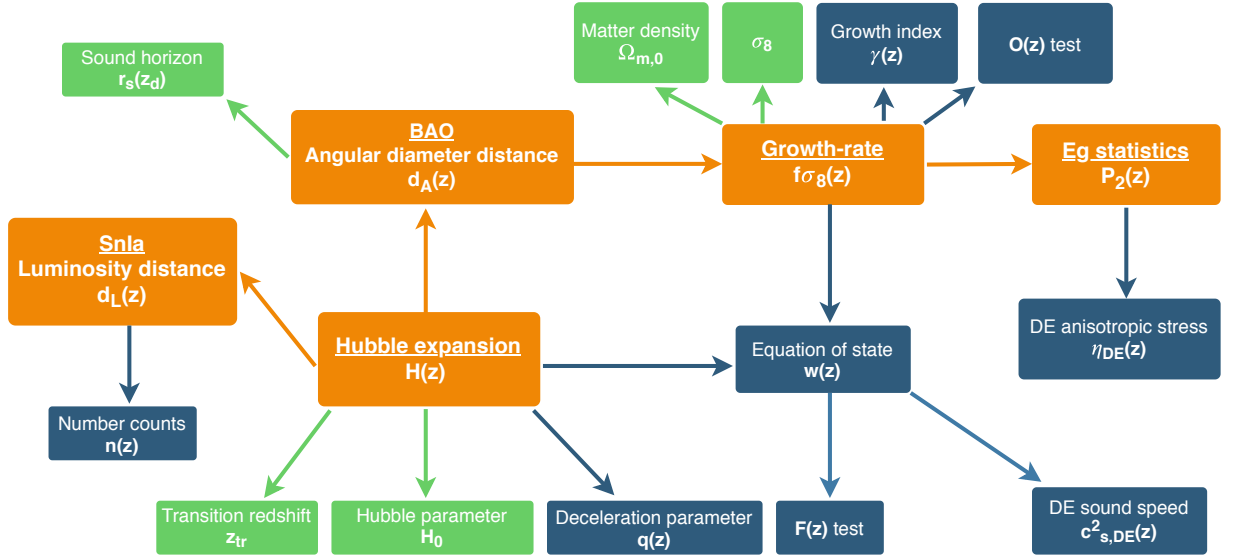


FIG. 1: A flowchart of the fitting process using the machine learning approach. The orange blocks represent primary quantities reconstructed directly from the data, i.e. the GA best-fits, the blue blocks represent quantities reconstructed from the latter, such as $w(z)$, and the green blocks stand for the derived (secondary) parameters. The flowchart shows the interplay between the different data and derived parameters, something which is reflected in our analysis.

a fiducial model, usually taken to be Λ CDM. However, specifically for the GP it was claimed in Ref. [57] that both of these choices do not influence the reconstruction.

As mentioned earlier, in order to reconstruct the data we will only make very few minimal physical or mathematical assumptions, but we will make no assumption of a DE model or that the spatial curvature of the Universe is zero, i.e. flatness. However, we will assume homogeneity, isotropy and the Friedmann-Robertson-Walker (FRW) metric. Specifically we have assumed:

1. The Hubble parameter today is given by the Hubble constant $H(z=0) = H_0$. Then, H_0 is estimated directly from the $H(z)$ data.
2. We assume the Hubble law at low redshifts $d_L(z \simeq 0) \simeq \frac{c}{H_0} z$. We use the Hubble constant H_0 from the $H(z)$ fit to break the degeneracies with the absolute SNIa magnitude.
3. Similarly, at low redshifts we assume $d_A(z \simeq 0) \simeq \frac{c}{H_0} z$ due to the Hubble law. We make no assumptions for the sound horizon at drag redshift r_d , which is minimized over. We again use the Hubble constant H_0 from the $H(z)$ fit.
4. The Universe at early times went through a phase of matter domination ($z \simeq 100$), so the linear growth behaves as $\delta_m(a) \simeq a$ at high redshifts.

We also note that the growth rate data has a dependence on the fiducial model which can be corrected by rescaling the measurements by the ratios of $H(z)D_A(z)$ as it is explained in Ref. [58]. Finally, the SNIa contain

some model dependence, as one must optimize parameters in the lightcurve function simultaneously with those of the assumed model. This mainly affects the covariance matrix, which is typically inferred based on an fiducial background model, usually Λ CDM. However, since in our case the best-fit is close to Λ CDM and the errors are much larger than the effects of the model-bias in the covariance, we can safely assume for now that these effects have a minimal effect to the minimization.

For illustration purposes we also present in Fig. 1 a flowchart of the whole fitting process, while the exact GA best-fits are given in Appendix C. To estimate the errors on these reconstructed quantities we use the *Path Integral* approach developed by Refs. [56, 59], where one calculates analytically a path integral over the whole functional space that can be scanned by the GA. Then this error is propagated onto the various derived quantities with the error propagation approach described in detail in Appendix D.

The flowchart of the fitting process shown in Fig. 1 highlights the interconnected nature of the data, something that was not taken into account in previous ML analyses [56, 59]. While this interplay complicates the analysis by adding potentially spurious correlations between the parameters, it also allows us to break degeneracies and constrain quantities in a model independent fashion, that previously was impossible, such as the anisotropic stress $\eta_{DE}(z)$.

III. RESULTS

We now present the main results of our analysis and specifically we show the reconstructions of several quantities including the DE equation of state $w_{DE}(z)$, the DE adiabatic sound speed $c_{s,DE}^2(z)$, the growth index $\gamma(z)$, the $\mathcal{O}(z)$ test, the DE anisotropic stress $\eta_{DE}(z)$, the number counts of luminous sources $n(z)$ and σ_8 , all of which are defined in Appendices A and B.

The actual GA fits used in the reconstructions and the derived parameters like Ω_{m0} etc, are shown in Appendix C, while in Table I we show the best-fit χ^2 for the GA functions versus those of the Λ CDM model. As we can see, in all cases the GA out-performs the Λ CDM model in the terms of the best-fit χ^2 .

In Fig. 2 we then show the DE equation of state $w(z)$ given by Eq. (B1) (left panel) and the adiabatic sound speed $c_{s,DE}^2$, where the latter is given by Eq. (B3). As can be seen, the equation of state $w(z)$ is consistent with Λ CDM at low redshifts, but shows a mild 2σ tension at $z \sim 1$, thus hinting that deviations from the Λ CDM could happen at higher redshifts as claimed in Ref. [11].

In the case of the adiabatic sound speed we focus on small redshifts as the earliest we can reconstruct it from the Hubble data is at $z > 0.07$. As we can see, in the range $z \in [0.07, 0.1]$ the adiabatic sound speed is evolving and is negative at the 2σ level, which implies that DE either has a dominant non-adiabatic component at small redshifts or it should have anisotropic stress, as otherwise the matter density perturbations would be unstable [25].

In Fig. 3 we show the growth index $\gamma(z)$ of the matter density perturbations (left panel) given by Eq. (B13) and the anisotropic stress $\eta_{DE}(z)$ (right panel) given by Eq. (A26). At low redshifts both parameters show deviations from their expected Λ CDM values (dashed lines) at a level of $\sim 3\sigma$ for the former and $\sim 3.5\sigma$ for the latter. At higher redshifts, $z \sim 1$ the growth index is consistent within the errors with Λ CDM while the anisotropic stress shows a $\sim 5.5\sigma$ deviation from unity.

Finally, in the left panel of Fig. 4 we also show the $\mathcal{O}(z)$ test of Refs. [49, 54] as defined in Eq. (B15), which we find is consistent with unity at all redshifts. On the right panel of Fig. 4 we show the number counts of luminous sources $n(z)$ given by Eq. (B4). In both cases, the dashed line corresponds to the theoretical prediction of the Λ CDM model, while the solid black line and the grey region to the GA best-fit and the 1σ errors. We find that the reconstructions agree with the Λ CDM model within the errors.

The deviations found in the DE anisotropic stress reconstructed from the E_g data and the DE equation of state $w(z)$ using the $H(z)$ data may hint either to unaccounted for systematics or new physics. For example, a potential source of the deviations observed with the E_g data may be due to the lensing magnification. In Refs. [60, 61] it was shown that lensing magnification modifies both the galaxy-galaxy lensing correlations and the galaxy-galaxy correlations. As a result, lensing mag-

TABLE I: The χ^2 for Λ CDM and GA using the growth $f\sigma_8$, the Hubble expansion $H(z)$, the Pantheon SnIa and Baryon Acoustic Oscillations (BAO) data.

| Model | $H(z)$ | SnIa | BAO | $f\sigma_8$ | P_2 |
|------------------------------|--------|----------|--------|-------------|--------|
| $\chi^2_{\Lambda\text{CDM}}$ | 19.476 | 1034.734 | 10.937 | 12.238 | 10.516 |
| χ^2_{GA} | 17.670 | 1034.030 | 8.091 | 12.220 | 5.422 |

nification both introduces systematic errors in the determination of E_g and makes it bias dependent. For a more in-depth discuss of the systematics see also [62].

IV. CONCLUSIONS

In summary, we find that there is a $\sim 2\sigma$ deviation of $w(z)$ from -1, the adiabatic sound speed $c_{s,DE}^2$ is evolving and is negative at the $\sim 2\sigma$ level, while using the E_g data we find a $\sim 3\sigma$ deviation of the anisotropic stress $\eta_{DE}(z)$ from unity at low redshifts and $\sim 3.5\sigma$ at high redshifts, thus suggesting the presence of significant deviations from the Λ CDM model.

Clearly, these inconsistencies present a problem as they hint towards two possibilities, either the presence of unaccounted for systematics, as might be the case for the E_g data, or new physics in the form of modifications of gravity. The latter case is quite plausible, the deviations come from very different data sets with very different systematics, i.e. the equation of state $w(z)$ and $c_{s,DE}^2$ from the $H(z)$ data, the growth index from the growth data coming from the RSD measurements and the $\eta_{DE}(z)$ from the E_g data.

Specifically, the fact that the adiabatic sound speed $c_{s,DE}^2$ is both evolving and negative, implies that the DE perturbations would be unstable unless there exists either a strong anisotropic stress, coming for example from some modification of gravity, so that the total effective sound speed is positive, as shown in Ref. [25] or a non-adiabatic DE component. In particular, using the effective fluid approach it can be shown that in $f(R)$ models, like the Hu-Sawicki or the designer model, the sound speed of the effective DE fluid is negative and the matter perturbations are stable due to the anisotropic stress [23], hence lending more support to modified gravity scenarios.

Finally, our analysis is completely agnostic as we made no assumptions about the nature of DE or the spatial curvature of the Universe during the fitting of our data. This is one of the main advantages of our ML approach compared to other traditional or non-parametric methods such as gaussian processes that assume a fiducial model or cosmography which suffers from convergence issues at high redshifts. As the GA can provide model-independent reconstructions of key parameters that describe DE, then if indeed there are no systematics in the data, the observed model-independent deviations from Λ CDM could point to the existence of new physics. The possibility of such an exciting prospect could be further

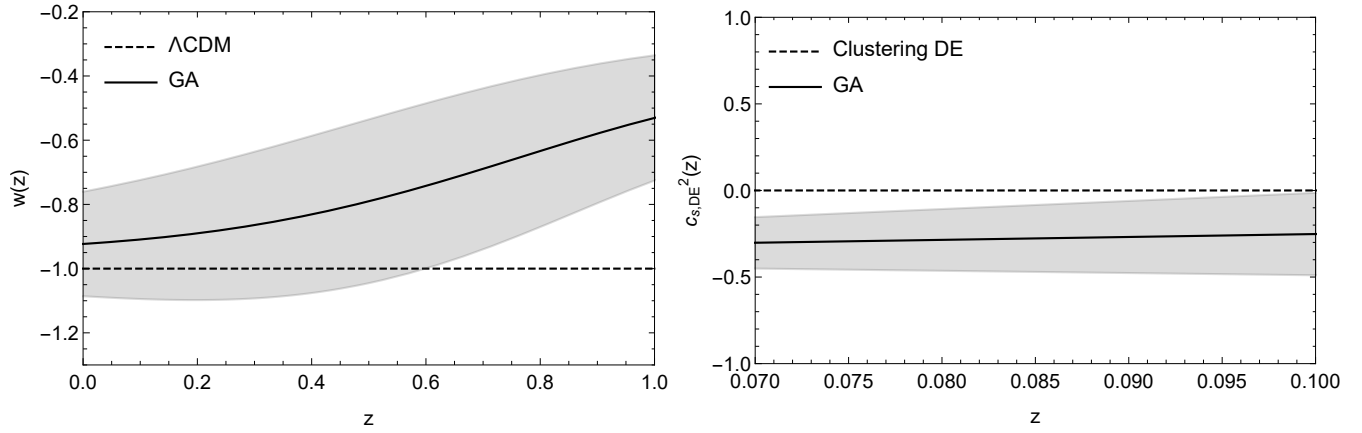


FIG. 2: Left: The DE equation of state $w(z)$ given by Eq. (B1), using the GA reconstruction of the Hubble data and the value of Ω_{m0} found from the growth data. We find that at high redshifts ($z \gtrsim 0.8$) there is a mild 2σ deviation from the Λ CDM model. The dashed line corresponds to the Λ CDM model, while the solid black line and the grey region to the GA best-fit and the 1σ errors. Right: The adiabatic DE sound speed $c_{s,DE}^2$ given by Eq. (B3). The dashed line corresponds to clustering DE with $c_s^2 = 0$, while the solid black line and the grey region to the GA best-fit and the 1σ errors. We focus on small redshifts as the earliest we can reconstruct it from the Hubble data is at $z > 0.07$ and in any case we are interested in deviations from Λ CDM at small redshifts.

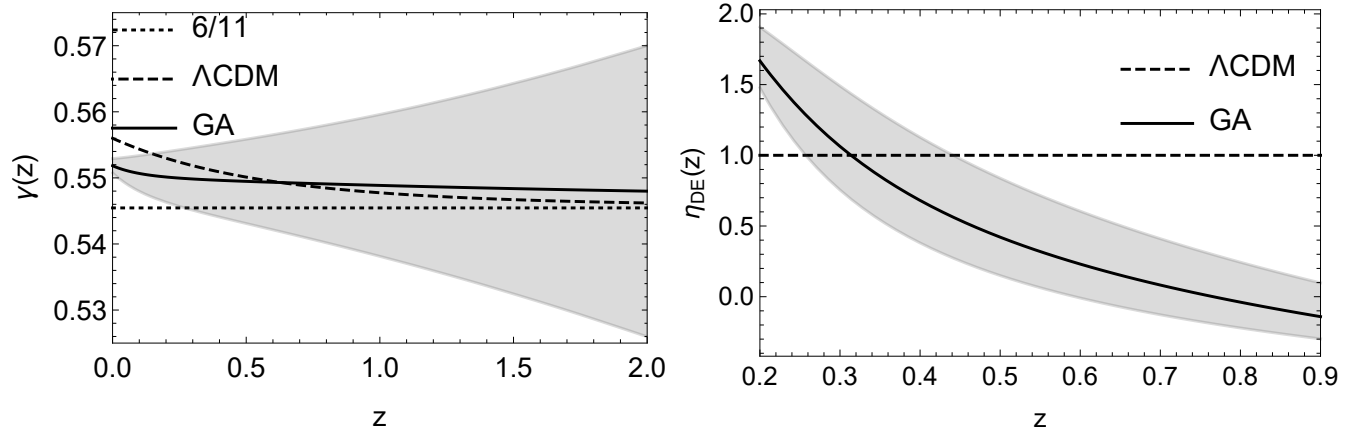


FIG. 3: Left: The growth index $\gamma(z)$ of the matter density perturbations given by Eq. (B13). The dashed line corresponds to the Λ CDM model, the dotted line to the rough estimate $\gamma \sim \frac{6}{11}$, while the solid black line and the grey region to the GA best-fit and the 1σ errors. We find that at small redshifts there is a $\sim 3\sigma$ deviation from the Λ CDM model. Right: The anisotropic stress parameter $\eta_{DE}(z)$ given by Eq. (A26). The dashed line corresponds to the Λ CDM model (no DE anisotropic stress), while the solid black line and the grey region to the GA best-fit and the 1σ errors. We find that there are deviations present at both low and high redshifts at the $\sim 3.5\sigma$ and $\sim 5.5\sigma$ level respectively.

strengthened by the upcoming cosmological surveys like LSST [37].

Data availability

Acknowledgements

The authors thank G. Ballesteros for useful discussions and acknowledge support from the Research Projects FPA2015-68048-03-3P [MINECO-FEDER], PGC2018-094773-B-C32 and the Centro de Excelencia Severo Ochoa Program SEV-2016-0597. S. N. also acknowledges support from the Ramón y Cajal program through Grant No. RYC-2014-15843.

The GA codes that were used to create the plots and other findings in our paper, will be made freely available upon publication of the paper at this URL.

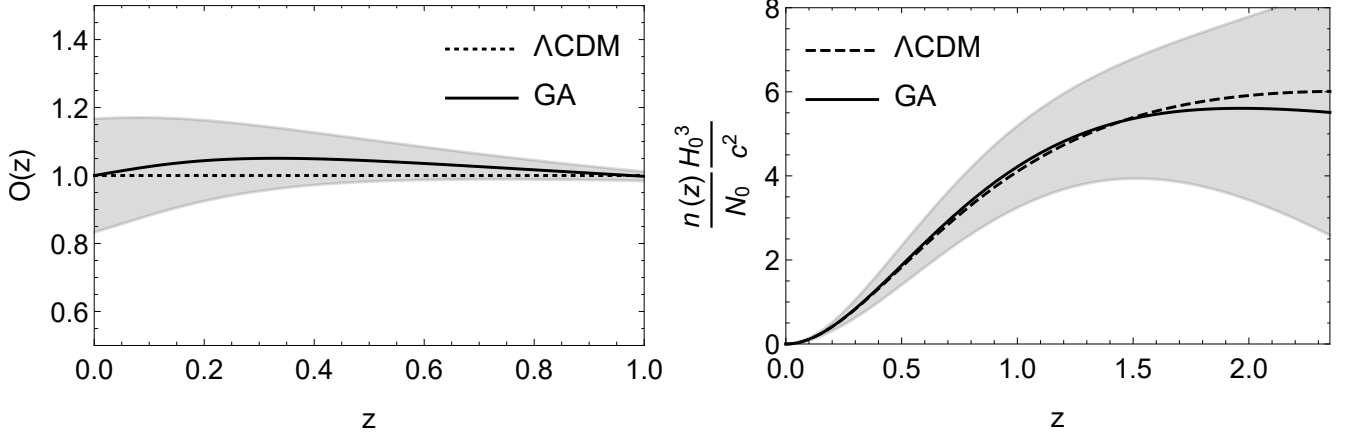


FIG. 4: Left: The $\mathcal{O}(z)$ test of Refs. [49, 54] given by Eq. (B15). The dashed line corresponds to the Λ CDM model (no DE anisotropic stress), while the solid black line and the grey region to the GA best-fit and the 1σ errors. We find that the test is consistent with Λ CDM within the errors. Right: The number counts of luminous sources given by Eq. (B4). The dashed line corresponds to the theoretical prediction of the Λ CDM model, while the solid black line and the grey region to the GA best-fit and the 1σ errors. We find that the reconstructions agree with the the Λ CDM model within the errors.

Appendix A: The data

1. $H(z)$ data

The Hubble expansion data are obtained in two complementary ways: by the clustering of galaxies or quasars and by the differential age method. The latter is connected to the redshift drift of distant objects over long time periods, usually a decade or longer, as in GR the Hubble parameter can also be expressed in terms of the time derivative of the redshift as $H(z) = -\frac{1}{1+z} \frac{dz}{dt}$ [63]. The former approach is connected to the clustering of quasars or galaxies and is a direct probe of the Hubble expansion by determining the BAO peak in the radial direction [64].

In this analysis we used the 36 points of the compilation from Ref. [23], which spans over a redshift range of $0.07 \leq z \leq 2.34$, where the data are in the form (z_i, H_i, σ_{H_i}) . We can minimize the χ^2 analytically over H_0 and the result is

$$\chi_H^2 = A - \frac{B^2}{\Gamma}, \quad (\text{A1})$$

$$H_0 = \frac{B}{\Gamma}, \quad (\text{A2})$$

where the parameters A , B and Γ are defined as

$$A = \sum_i^{N_H} \left(\frac{H_i}{\sigma_{H_i}} \right)^2, \quad (\text{A3})$$

$$B = \sum_i^{N_H} \frac{H_i E^{th}(z_i)}{\sigma_{H_i}^2}, \quad (\text{A4})$$

$$\Gamma = \sum_i^{N_H} \left(\frac{E^{th}(z_i)}{\sigma_{H_i}} \right)^2, \quad (\text{A5})$$

while we denote the theoretical value of the Hubble parameter as $E^{th}(z) = H^{th}(z)/H_0$ and we set $N_H = 36$.

The aforementioned data can be used to measure the Hubble constant H_0 , determine the deceleration transition redshift but also to constrain the spatial curvature of the Universe along with distance redshift data, but also the non-relativistic matter and DE parameters, as shown in [65]. The Hubble constant H_0 has been the focus of an extended discussion in the literature, in light of a tension between local and high-redshift measurements of the parameter, see Ref. [9, 10] and references there in for a recent discussion.

2. Supernovae Type Ia data

We use the Pantheon SnIa compilation of Ref. [66] of 1048 Supernovae Ia points in the redshift range $0.01 < z < 2.26$ along with their covariances. The apparent magnitude m_B is

$$m_B = 5 \log_{10} \left(\frac{d_L(z)}{1 \text{ Mpc}} \right) + 25 + M_B, \quad (\text{A6})$$

where $d_L(z)$ is the luminosity distance and M_B the absolute magnitude. We then marginalize over the nuisance parameter M_B , as shown in the Appendix C of Ref. [67]. Then our final expression for the χ^2 is

$$\chi_{SnIa}^2 = A - \frac{B^2}{E} + \ln \left(\frac{E}{2\pi} \right), \quad (\text{A7})$$

where $A = \Delta \vec{m} \cdot \mathbf{C}^{-1} \cdot \Delta \vec{m}$, $B = \Delta \vec{m} \cdot \mathbf{C}^{-1} \cdot \Delta \vec{l}$ and $E = \vec{l} \cdot \mathbf{C}^{-1} \cdot \vec{l}$, while \mathbf{C} is the SnIa covariance matrix, $\vec{l} = (1, 1, \dots, 1)$ and $\Delta m \equiv m_{B,i} - m_{th}(z_i)$.

3. Baryon Acoustic Oscillations

We use the BAO data from 6dFGS [68], SDDS [69], BOSS CMASS [70], WiggleZ [71], MGS [72] and BOSS DR12 [73], DES [74], Lya [75], DR - 14 LRG [76] and quasars [77]. To facilitate the description of the data, we define the following functions:

$$d_z \equiv \frac{r_s(z_d)}{D_V(z)}, \quad (\text{A8})$$

where the sound speed is $r_s(z_d) = \frac{c}{H_0} \int_{z_d}^{\infty} \frac{c_s(z)}{H(z)/H_0} dz$ where z_d is the redshift at the dragging epoch, see Eq. (4) of Hu [78], and in the Λ CDM model the sound horizon can be approximated by

$$r_s(z_d) \simeq \frac{44.5 \log\left(\frac{9.83}{\Omega_{m0} h^2}\right)}{\sqrt{1 + 10(\Omega_{b0} h^2)^{3/4}}} \text{Mpc/h}. \quad (\text{A9})$$

Also, we need the functions

$$D_V(z) = \left[(1+z)^2 d_A(z)^2 \frac{cz}{H(z)} \right]^{1/3}. \quad (\text{A10})$$

and

$$D_H(z) = c/H(z). \quad (\text{A11})$$

Then the 6dFGs and WiggleZ BAO data are given by

| z | d_z | σ_{d_z} |
|-------|--------|----------------|
| 0.106 | 0.336 | 0.015 |
| 0.44 | 0.073 | 0.031 |
| 0.6 | 0.0726 | 0.0164 |
| 0.73 | 0.0592 | 0.0185 |

(A12)

and their inverse covariance matrix by

$$C_{ij}^{-1} = \begin{pmatrix} \frac{1}{0.015^2} & 0 & 0 & 0 \\ 0 & 1040.3 & -807.5 & 336.8 \\ 0 & -807.5 & 3720.3 & -1551.9 \\ 0 & 336.8 & -1551.9 & 2914.9 \end{pmatrix} \quad (\text{A13})$$

with the χ^2 given by

$$\chi_{6dFS,Wig}^2 = V^i C_{ij}^{-1} V^j, \quad (\text{A14})$$

and $V^i = d_{z,i} - d_z(z_i, \Omega_{m0})$.

The BAO measurements for MGS and SDSS (Lowz and Cmass) are given by $D_V/r_s = 1/d_z$ via

| z | $1/d_z$ | σ_{1/d_z} |
|------|---------|------------------|
| 0.15 | 4.46567 | 0.168135 |
| 0.32 | 8.62 | 0.15 |
| 0.57 | 13.7 | 0.12 |

(A15)

and the

$$\chi_{MGS,SDSS}^2 = \sum \left(\frac{1/d_{z,i} - 1/d_z(z_i, \Omega_{m0})}{\sigma_{1/d_{z,i}}} \right)^2. \quad (\text{A16})$$

The BAO data from DES is of the form $d_A(z)/r_s$ with $(z, d_A(z)/r_s, \sigma) = (0.81, 10.75, 0.43)$ and the χ^2 given by

$$\chi_{DES}^2 = \sum \left(\frac{d_A(z,i)/r_s - d_A(z_i, \Omega_{m0})/r_s}{\sigma_{d_A(z,i)/r_s}} \right)^2. \quad (\text{A17})$$

The BAO data from Lya are of the form $f_{BAO} = (d_A/r_s, D_H/r_s)$ and are given by

| z | f_{BAO} | $\sigma_{f_{BAO}}$ |
|------|-----------|--------------------|
| 2.35 | 36.3 | 1.8 |
| 2.35 | 9.2 | 0.36 |

(A18)

with the χ^2 given by

$$\chi_{Lya}^2 = \sum \left(\frac{f_{BAO,i} - f_{BAO}(z_i, \Omega_{m0})}{\sigma_{f_{BAO}}} \right)^2. \quad (\text{A19})$$

Finally, the DR-14 LRG and quasars BAO data assume $r_{s,fid} = 147.78$ Mpc/h and are given by $D_V/r_s = 1/d_z$

| z | $1/d_z$ | σ_{1/d_z} |
|------|--------------------------|-------------------------|
| 0.72 | $\frac{2353}{r_{s,fid}}$ | $\frac{62}{r_{s,fid}}$ |
| 1.52 | $\frac{3843}{r_{s,fid}}$ | $\frac{147}{r_{s,fid}}$ |

(A20)

and the χ^2 given by

$$\chi_{LRG,Q}^2 = \sum \left(\frac{1/d_{z,i} - 1/d_z(z_i, \Omega_{m0})}{\sigma_{1/d_{z,i}}} \right)^2. \quad (\text{A21})$$

The total χ^2 is then

$$\chi_{tot}^2 = \chi_{6dFS,Wig}^2 + \chi_{MGS,SDSS}^2 + \chi_{DES}^2 + \chi_{Lya}^2 + \chi_{LRG,Q}^2. \quad (\text{A22})$$

All the χ^2 terms in the previous equation depend on the sound speed at the drag redshift $r_d = r_s(z_d)$ via Eq. (A8), which is difficult to estimate in a model independent approach. Therefore, we leave r_d as a free parameter and obtain its value from the data by minimize the χ^2 over it.

4. Growth data

We also use the growth-rate $f\sigma_8$ compilation given in Table I of Ref. [79], where the authors analyzed different subsets in the data and implemented Bayesian model comparison to test the internal robustness of the dataset. These data are obtained via the redshift-space distortions and in fact determine the combination $f\sigma_8(a) \equiv f(a) \cdot \sigma(a)$, where $f(a) = \frac{d \ln \delta_m}{d \ln a}$ is the growth rate, $\sigma(a) = \sigma_{8,0} \frac{\delta_m(a)}{\delta_m(1)}$ is the rms fluctuation of the linear density field within spheres of radius $R = 8h^{-1} \text{Mpc}$, while $\sigma_{8,0}$ is the value of this parameter today.

The value of $f\sigma_8(a)$ can be directly determined from the ratio of the monopole to the quadrupole of the redshift-space power spectrum, which depends on the parameter $\beta = f/b_0$, where b_0 is the bias and f is the growth rate assuming linear theory [80–82]. It can be shown that $f\sigma_8(a)$ is independent of the bias, as the latter completely cancels out from the previous expression.

Moreover, $f\sigma_8(a)$ has been shown to be a good discriminator of DE models [81]. For more details on the covariance matrix of the data and how to correct for the Alcock-Paczynski effect see Refs. [79], [58] and [83]. The advantage of using the combination $f\sigma_8$, instead of just the growth-rate $f(z)$, is that the former is directly associated to the power spectrum of peculiar velocities of galaxies [84].

5. E_g data

The flat Friedmann-Robertson-Walker (FRW) metric, which can describe accurately the geometry of the Universe, reads $ds^2 = -(1+2\Psi)dt^2 + a(t)^2(1-2\Phi)dx^2$, where a is the scale factor and Ψ and Φ are two scalar gravitational potentials. Then the gravitational slip, can be defined as the ratio of the gravitational potentials $\eta_{DE} = \frac{\Phi}{\Psi}$, which in GR is equal to unity. These potentials satisfy the two Poisson equations in Fourier space:

$$-\frac{k^2}{a^2}(\Phi + \Psi) = 4\pi G_N \Sigma(k, a) \rho_m \delta_m, \quad (\text{A23})$$

$$-\frac{k^2}{a^2}\Psi = 4\pi G_N \mu(k, a) \rho_m \delta_m, \quad (\text{A24})$$

where G_N is the bare Newton's constant, while Σ and μ parameterize deviations in GR. In the case of the latter, $\Sigma = 2$ and $\mu = 1$.

In order to test the aforementioned relations, the E_g statistic was created, aiming for it to be bias independent at linear order [85, 86]. The E_g test can be expressed as the expectation value of the ratio of lensing and galaxy clustering observables at a scale k as follows

$$E_g = \left\langle \frac{a \nabla^2 (\Psi + \Phi)}{3H_0^2 f \delta_m} \right\rangle. \quad (\text{A25})$$

To derive the gravitational slip in a model independent way we reconstruct two quantities through the E_g and $f\sigma_8$ data. The first quantity is $P_2(z)$ which is defined as $P_2 = \frac{\Omega_{m0}\Sigma}{f}$ and depends on the lensing potential and the growth rate. In GR this reduces to $P_2 = \frac{2\Omega_{m0}}{f}$ which implies that in GR we have $E_g = \frac{\Omega_{m0}}{f}$. In general, E_g can be related to the P_2 statistic of Ref. [87] via $P_2 = 2E_g$. The second quantity is P_3 , expressed as $P_3 = \frac{(f\sigma_8(z))'}{f\sigma_8(z)}$, where the tilde is the derivative with respect to $\ln a$.

Then, the gravitational slip can be derived in a model independent way as [87]

$$\eta_{DE}(z) = \frac{3P_2(z)(1+z)^3}{2E(z)^2 \left(P_3(z) + 2 + \frac{E'(z)}{E(z)} \right)} - 1, \quad (\text{A26})$$

where $E(z) = H(z)/H_0$. The exact data points we used are given in Table II for completeness.

TABLE II: The E_g data used in this analysis as compiled by Refs. [87] and [62]. Note that some of the points in the previous references were duplicates as they come from the same surveys, albeit with combinations of different external probes, so we use only one of the measurements to avoid strong correlations.

| z | E_g | σ_{E_g} |
|-------|-------|----------------|
| 0.267 | 0.43 | 0.13 |
| 0.305 | 0.27 | 0.08 |
| 0.320 | 0.40 | 0.09 |
| 0.554 | 0.26 | 0.07 |
| 0.570 | 0.31 | 0.06 |
| 0.570 | 0.30 | 0.07 |
| 0.600 | 0.16 | 0.09 |
| 0.860 | 0.09 | 0.07 |

Appendix B: Supplemental theoretical material

In this Appendix we present some supplemental theoretical material regarding the quantities reconstructed in the main text. The DE equation of state $w(z) \equiv \frac{P}{\rho}$ and the deceleration parameter $q(z) \equiv -\frac{\ddot{a}}{aH(a)^2}$ can be written as [88]

$$w(z) = -1 + \frac{1}{3}(1+z) \frac{d \ln(\Omega_{DE}(z))}{dz}, \quad (\text{B1})$$

$$q(z) = -1 + (1+z) \frac{d \ln(H(z))}{dz}, \quad (\text{B2})$$

where $\Omega_{DE}(z) \equiv H(z)^2/H_0^2 - \Omega_{m,0}(1+z)^3$ is the DE energy density. When $w(z) = -1$ we recover the Λ CDM model, for which $q_0 = q(z=0) = -1 + \frac{3\Omega_{m0}}{2}$. Here and in what follows we will neglect radiation as it is negligible at late times when we perform our GA reconstructions.

We also constrain the DE adiabatic sound speed $c_{s,DE}^2(z)$. The latter can be written in terms of the DE equation of state $w(z)$ as

$$\begin{aligned} c_{s,DE}^2(z) &= \frac{\delta P_{DE}}{\delta \rho_{DE}} \\ &\simeq w(z) + \frac{1+z}{3} \frac{w'(z)}{1+w(z)}. \end{aligned} \quad (\text{B3})$$

We also consider the number counts of luminous sources, which are given by [89]

$$n(z) = \frac{4\pi \mathcal{N}_0 d_L(z)^2}{H(z)(1+z)^2}, \quad (\text{B4})$$

where $\mathcal{N}_0 \equiv \int_0^\infty \mathcal{N}_0(L) dL$ is the total number of sources per proper volume integrated over all luminosities.

Next we also consider variables related to the matter density perturbations. One of the most interesting such

variables is the growth index of matter density perturbations $\gamma(a)$, which is defined via [90]

$$f(a) = \Omega_m(a)^{\gamma(a)}, \quad (\text{B5})$$

where $f(a) = \frac{d \ln \delta_m}{d \ln a}$ is the logarithmic derivative of the growth of matter perturbations $\delta_m(a) \equiv \frac{\delta \rho_m}{\rho_m}$, the matter density is given by $\Omega_m(a) = \frac{\Omega_{m0} a^{-3}}{H(a)^2/H_0^2}$ and $H(a) \equiv \frac{\dot{a}}{a}$, is the Hubble parameter as a function of the dimensionless scale factor $a = \frac{1}{1+z}$ that describes the expansion of the universe. Solving for the growth index we find that it can be expressed as

$$\begin{aligned} \gamma(a) &= \frac{\ln(f(a))}{\ln(\Omega_m(a))} \\ &= \frac{\ln(f(a))}{\ln\left(\frac{\Omega_{m0} a^{-3}}{H(a)^2/H_0^2}\right)}. \end{aligned} \quad (\text{B6})$$

We can now proceed to reexpress the various quantities contained in Eq. (B6) with ones that can be reconstructed directly from the data. Assuming a homogeneous and isotropic universe in GR, with no DE perturbations and neglecting neutrinos, which we can do as our data are not in such small scales affected by them, then the growth factor $\delta_m(a)$ satisfies the differential equation:

$$\delta_m''(a) + \left(\frac{3}{a} + \frac{H'(a)}{H(a)}\right) \delta_m'(a) - \frac{3}{2} \frac{\Omega_{m0}}{a^5 H(a)^2/H_0^2} \delta_m(a) = 0. \quad (\text{B7})$$

However, what is measurable is not exactly the growth $\delta_m(a)$, but the combination

$$\begin{aligned} f\sigma_8(a) &\equiv f(a) \cdot \sigma(a) \\ &= \frac{\sigma_8}{\delta_m(1)} a \delta_m'(a), \end{aligned} \quad (\text{B8})$$

where $f(a)$ is the growth rate and $\sigma(a) = \sigma_8 \frac{\delta_m(a)}{\delta_m(1)}$ is the redshift-dependent rms fluctuations of the linear density field at $R = 8h^{-1}\text{Mpc}$ while the parameter σ_8 is its value today. The combination of $f\sigma_8(a)$ is bias-free as both $f(a)$ and $\sigma_8(a)$ have a dependence on bias which is the inverse of the other, thus cancels out, and it has been shown to be a good discriminator of DE models [81].

Performing direct manipulations of the definition of $f\sigma_8$ of Eq. (B7) and Eq. (B8) one can show, see also Ref. [91], that

$$\begin{aligned} \frac{\delta_m(a)}{\delta_m(1)} &= \frac{1}{\sigma_8} \int_0^a \frac{f\sigma_8(x)}{x} dx \\ H(a)^2/H_0^2 &= \frac{3\Omega_{m0}}{a^4 f\sigma_8(a)^2} \int_0^a dx f\sigma_8(x) \int_0^x dy \frac{f\sigma_8(y)}{y}, \end{aligned} \quad (\text{B9})$$

but also the useful relations:

$$\sigma_8 = \int_0^1 \frac{f\sigma_8(x)}{x} dx \quad (\text{B11})$$

$$\Omega_{m0} = \frac{1}{3 \int_0^1 dx \frac{f\sigma_8(x)}{f\sigma_8(1)} \int_0^x dy \frac{1}{y} \frac{f\sigma_8(y)}{f\sigma_8(1)}}. \quad (\text{B12})$$

Combining Eqs. (B6) and (B9)-(B10), we obtain our main result for the growth index:

$$\gamma(a) = \frac{\ln\left(\frac{f\sigma_8(a)}{\int_0^a \frac{f\sigma_8(x)}{x} dx}\right)}{\ln\left(\frac{af\sigma_8(a)^2}{3 \int_0^a dx f\sigma_8(x) \int_0^x dy \frac{f\sigma_8(y)}{y}}\right)}. \quad (\text{B13})$$

The main advantages of Eq. (B13) are that it only requires knowledge of $f\sigma_8(a)$ and does not depend on Ω_{m0} or $H(a)$, σ_8 or any other parameter.

Finally, exploiting the Noether symmetries of Eq. (B7) we can define a conserved charge that has to be constant at all times and redshifts, thus is an ideal null test. Following this procedure, Ref. [54] showed that the null test can be written as

$$\mathcal{O}(z) = a^2 E(a) \frac{f\sigma_8(a)}{f\sigma_8(1)} e^{I(z)}, \quad (\text{B14})$$

$$I(z) = -\frac{3}{2} \Omega_{m0} \int_1^a \frac{\sigma_{80} + \int_1^x \frac{f\sigma_8(y)}{y} dy}{x^4 E(x)^2 f\sigma_8(x)} dx, \quad (\text{B15})$$

where we rewrite $\sigma_{80} = \sigma_8(a=1)$ for simplicity and we have set $E(a) \equiv \frac{H(a)}{H_0}$. It is clear that Eq. (B15) has to be constant for all redshifts z and moreover $\mathcal{O}(z)$ has to be equal to 1 and any deviation from unity might hint towards a deviation from the FLRW Universe, non zero DE perturbations, a deviation from GR or a tension between the $H(z)$ and $f\sigma_8$ data.

Appendix C: GA results

Applying the GA to the cosmological data described in Appendix A we find the following best-fit functions

$$H(z) = H_0 \left(1 + z(-0.676 - 0.221z + 0.018z^3)\right), \quad (\text{C1})$$

$$d_L(z) = \frac{c}{H_0} z \left(1 + z(0.872 - 0.133z - 0.002z^2)\right), \quad (\text{C2})$$

$$d_A(z) = \frac{c}{H_0} z \left(1 - z(0.0014 + 0.013z)^{-0.019+0.135z}\right), \quad (\text{C3})$$

$$f\sigma_8(a) = f_0 \left(a - a^4(1.629 - 0.848a + 0.024a^{3.50})\right), \quad (\text{C4})$$

$$P_2(a) = (-0.839a - 0.559a^2 e^{-0.4136a})^2, \quad (\text{C5})$$

where $H_0 = 68.5019 \text{ km/s/Mpc}$ and $f_0 = 1.05749$. Inserting our reconstructed functions in Eqs. (B11), (B12) and (B13) we derived the following constraints

$$\sigma_8 = 0.808 \pm 0.251, \quad (\text{C6})$$

$$\Omega_{m0} = 0.247 \pm 0.032, \quad (\text{C7})$$

$$\gamma_0 = 0.552 \pm 0.001. \quad (\text{C8})$$

From the BAO data we obtain

$$r_d = 150.811 \pm 0.365 \text{ Mpc/h}, \quad (\text{C9})$$

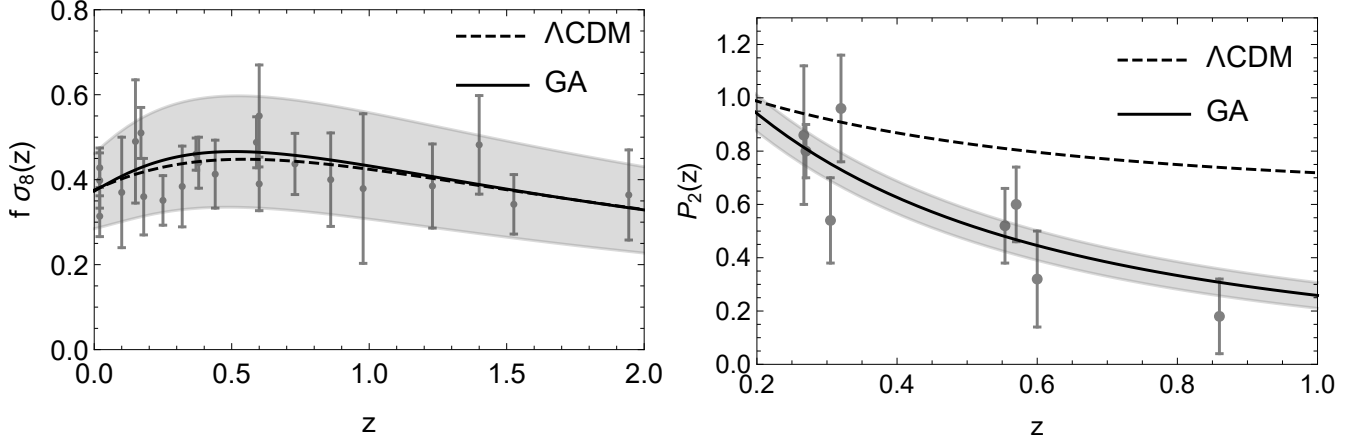


FIG. 5: Left: The $f\sigma_8$ data compilation along with the Λ CDM best-fit (green line) and the GA best-fit (solid black line). Right, the P_2 parameter of [87] along with the E_g data given in Table II.

while from the $H(z)$ data we get

$$H_{GA,0} = 68.502 \pm 11.434 \text{ km/s/Mpc}, \quad (\text{C10})$$

$$w_{GA,0} = -0.923 \pm 0.104, \quad (\text{C11})$$

$$q_{GA,0} = -0.543 \pm 0.118, \quad (\text{C12})$$

$$z_{GA,tr} = 0.641 \pm 0.023. \quad (\text{C13})$$

For completeness we show in the left panel of Fig. 5 the $f\sigma_8$ data compilation along with the Λ CDM best-fit (green line) and the GA best-fit (solid black line), while in the right panel we show the P_2 parameter of [87] along with the E_g data given in Table II.

Appendix D: Error analysis

Here we describe the analysis we used for the propagation of errors, given our unique non-parametric approach. If we have a function $f(x)$ that is reconstructed by the GA approach, then the GA approach will give us the best-fit $f_{GA}(x)$ and the 1σ error $\delta f(x)$. Then, as the GA evolves, we can treat the values of the function f as random variables described by a normal distribution

$$\mathcal{L}(f) = \frac{e^{-\frac{(f-f_{GA})^2}{2\delta f^2}}}{\sqrt{2\pi}\delta f}. \quad (\text{D1})$$

Then the error propagated to any quantity formed by the function f , eg $g = g(f)$ can be estimated by using the definition of the standard deviation $\delta g^2 = \langle g^2 \rangle - \langle g \rangle^2$ and the expectation value $\langle g \rangle = \int_{-\infty}^{+\infty} g(f) \mathcal{L}(f) df$. For example, we demonstrate this approach for the simple example of $g(f) = f^2$, where we would expect the error of g to be $\delta g = 2f_{GA}\delta f + \dots$. Indeed, we find

$$\begin{aligned} \langle g^2 \rangle &= 3\delta f^4 + f_{GA}^4 + 6\delta f^2 f_{GA}^2 \\ \langle g \rangle^2 &= (\delta f^2 + f_{GA}^2)^2, \end{aligned} \quad (\text{D2})$$

which gives

$$\begin{aligned} \delta g &= \sqrt{2\delta f^4 + 4\delta f^2 f_{GA}^2} \\ &\simeq 2f_{GA}\delta f + \dots, \end{aligned} \quad (\text{D3})$$

in agreement with the expected value. Similarly, one can derive for example the error of the Om statistic, which can be reconstructed using the GA best-fit $H_{GA}(z)$ [47]. Noting that the Om statistic is defined as

$$Om(z) = \frac{H(z)^2/H_0^2 - 1}{(1+z)^3 - 1}, \quad (\text{D4})$$

then, using the aforementioned approach we find the error on the Om statistic is

$$\delta Om(z) = \frac{2H_{GA}(z)\delta H(z)/H_0^2}{(1+z)^3 - 1}, \quad (\text{D5})$$

as expected for traditional error propagation.

Similarly, one can derive the error propagation of a quantity that depends on two reconstructed quantities by the GA. The procedure is exactly the same as before and we now consider the example of the DE energy density parameter $\Omega_{DE} = \frac{H(z)^2}{H_0^2} - \Omega_{m0}(1+z)^3$, where we assume the two reconstructed quantities are $H(z)$ and Ω_{m0} , each being described by a normal distribution. In this case the error on Ω_{DE} can be found to be:

$$\delta\Omega_{DE}(z)^2 \simeq 4\frac{H(z)^2}{H_0^2}\frac{\delta H(z)^2}{H_0^2} + (1+z)^6\delta\Omega_{m0}^2 + \dots, \quad (\text{D6})$$

again in agreement with the expected value from standard error propagation.

We also have to calculate quantities the contain derivatives, such as the DE equation of state or the deceleration parameter. In this case we will assume that we can model the error propagation as a variation of the functions during the evolution of the functional space of the

GA, i.e. $\delta f = \delta(f)$. This is in agreement with the previous approach as if we assume $g = f^2$ then $\delta g = 2f\delta f$ as expected.

Then we further assume that the variational δ commutes with derivatives, i.e. $\delta(\frac{df}{dx}) = \frac{d}{dx}(\delta f(x))$. The reason for this is that we can always assume that at any point x functions f that are close to the best-fit, can be written as $f \simeq f_{GA} + \delta f$, so that $\frac{df}{dx} \simeq \frac{df_{GA}}{dx} + \frac{d\delta f}{dx}$, which implies $\delta(\frac{df}{dx}) \simeq \frac{df}{dx} - \frac{df_{GA}}{dx} \simeq \frac{d\delta f}{dx}$ as mentioned before.

For example, in the case of the deceleration parameter we have:

$$q_{GA}(z) = -1 + (1+z) \frac{d \ln H_{GA}}{dz} \quad (D7)$$

which implies that the error is

$$\begin{aligned} \delta q &= (1+z) \delta \left[\frac{d \ln H}{dz} \right] \\ &= (1+z) \frac{d}{dz} [\delta \ln H] \\ &= (1+z) \frac{d}{dz} \left[\frac{\delta H}{H_{GA}} \right]. \end{aligned} \quad (D8)$$

Similarly, we will assume that the variational δ commutes with integrals, so that for example for the σ_8 parameter we have:

$$\sigma_{8,GA} = \int_0^1 \frac{f\sigma_{8,GA}}{x} dx \quad (D9)$$

and the corresponding error on the derived GA best-fit is

$$\delta\sigma_8 = \int_0^1 \frac{\delta f\sigma_8}{x} dx. \quad (D10)$$

Similarly, for the matter density parameter Ω_{m0} we have

$$\begin{aligned} \Omega_{m,0GA} &= \frac{1}{3 \int_0^1 dx \frac{f\sigma_{8GA}(x)}{f\sigma_{8GA}(1)} \int_0^x dy \frac{1}{y} \frac{f\sigma_{8GA}(y)}{f\sigma_{8GA}(1)}} \\ &= \frac{1}{3 \int_0^1 dx F(x) \int_0^x dy \frac{1}{y} F(y)}, \end{aligned} \quad (D11)$$

where $F(x) = \frac{f\sigma_{8GA}(x)}{f\sigma_{8GA}(1)}$. Then, the error is

$$\frac{\delta\Omega_{m,0}}{3\Omega_{m,0}^2} = \left| \int_0^1 dx \left[\delta F(x) \int_0^x dy \frac{F(y)}{y} + F(x) \int_0^x dy \frac{\delta F(y)}{y} \right] \right|, \quad (D12)$$

where we have set

$$\begin{aligned} \delta F(a) &= \delta \left(\frac{f\sigma_8(a)}{f\sigma_8(1)} \right) \\ &= \frac{\delta f\sigma_8(a)}{f\sigma_{8GA}(1)} - \frac{f\sigma_{8GA}(a)}{f\sigma_{8GA}(1)^2} \delta f\sigma_8(1). \end{aligned} \quad (D13)$$

-
- [1] A. G. Riess et al. (Supernova Search Team), *Astron. J.* **116**, 1009 (1998), astro-ph/9805201.
 - [2] S. Perlmutter et al. (Supernova Cosmology Project), *Astrophys. J.* **517**, 565 (1999), astro-ph/9812133.
 - [3] N. Aghanim et al. (Planck) (2018), 1807.06209.
 - [4] A. G. Riess, S. Casertano, W. Yuan, L. M. Macri, and D. Scolnic, *Astrophys. J.* **876**, 85 (2019), 1903.07603.
 - [5] M. Benetti and S. Capozziello (2019), 1910.09975.
 - [6] T. M. C. Abbott et al. (DES), *Mon. Not. Roy. Astron. Soc.* **480**, 3879 (2018), 1711.00403.
 - [7] J. W. Henning et al. (SPT), *Astrophys. J.* **852**, 97 (2018), 1707.09353.
 - [8] V. Bonvin et al., *Mon. Not. Roy. Astron. Soc.* **465**, 4914 (2017), 1607.01790.
 - [9] A. G. Riess, *Nature Rev. Phys.* **2**, 10 (2019), 2001.03624.
 - [10] P. Lemos, E. Lee, G. Efstathiou, and S. Gratton, *Mon. Not. Roy. Astron. Soc.* **483**, 4803 (2019), 1806.06781.
 - [11] G. Risaliti and E. Lusso, *Nat. Astron.* **3**, 272 (2019), 1811.02590.
 - [12] E. Di Valentino, A. Melchiorri, and J. Silk, *Nat. Astron.* (2019), 1911.02087.
 - [13] H. Velten and S. Gomes (2019), 1911.11848.
 - [14] E. Di Valentino, A. Melchiorri, O. Mena, and S. Vagnozzi (2019), 1910.09853.
 - [15] W. Lin, K. J. Mack, and L. Hou (2019), 1910.02978.
 - [16] D. Camarena and V. Marra (2019), [Phys. Rev. Research.2,013028(2020)], 1906.11814.
 - [17] W. Handley and P. Lemos, *Phys. Rev.* **D100**, 043504 (2019), 1902.04029.
 - [18] S. Gariazzo, in *15th Marcel Grossmann Meeting on Recent Developments in Theoretical and Experimental General Relativity, Astrophysics, and Relativistic Field Theories (MG15) Rome, Italy, July 1-7, 2018* (2018), 1812.00638.
 - [19] R.-Y. Guo, J.-F. Zhang, and X. Zhang, *JCAP* **1902**, 054 (2019), 1809.02340.
 - [20] T. Clifton, P. G. Ferreira, A. Padilla, and C. Skordis, *Phys. Rept.* **513**, 1 (2012), 1106.2476.
 - [21] D. Huterer, *Gen. Rel. Grav.* **42**, 2177 (2010), 1001.1758.
 - [22] W. Cardona, R. Arjona, and S. Nesseris (2019), 1907.10130.
 - [23] R. Arjona, W. Cardona, and S. Nesseris, *Phys. Rev.* **D99**, 043516 (2019), 1811.02469.
 - [24] R. Arjona, W. Cardona, and S. Nesseris, *Phys. Rev.* **D100**, 063526 (2019), 1904.06294.
 - [25] W. Cardona, L. Hollenstein, and M. Kunz, *JCAP* **1407**, 032 (2014), 1402.5993.
 - [26] T. Koivisto and D. F. Mota, *Phys. Rev.* **D73**, 083502 (2006), astro-ph/0512135.
 - [27] D. F. Mota, J. R. Kristiansen, T. Koivisto, and N. E. Groeneboom, *Mon. Not. Roy. Astron. Soc.* **382**, 793 (2007), 0708.0830.
 - [28] V. C. Busti and C. Clarkson, *JCAP* **1605**, 008 (2016), 1505.01821.
 - [29] F. O. Franco, C. Bonvin, and C. Clarkson (2019), 1906.02217.

- [30] Y. Akrami et al. (Planck) (2018), 1807.06205.
- [31] S. Basilakos and S. Nesseris, Phys. Rev. **D96**, 063517 (2017), 1705.08797.
- [32] C. I. Luna, S. Basilakos, and S. Nesseris, Phys. Rev. **D98**, 023516 (2018), 1805.02926.
- [33] S. Nesseris, Phys. Rev. **D88**, 123003 (2013), 1309.1055.
- [34] A. de la Cruz-Dombriz and A. Dobado, Phys. Rev. **D74**, 087501 (2006), gr-qc/0607118.
- [35] T. Multamaki and I. Vilja, Phys. Rev. **D73**, 024018 (2006), astro-ph/0506692.
- [36] L. Pogosian and A. Silvestri, Phys. Rev. **D77**, 023503 (2008), [Erratum: Phys. Rev. **D81**, 049901 (2010)], 0709.0296.
- [37] P. A. Abell et al. (LSST Science, LSST Project) (2009), 0912.0201.
- [38] T. M. C. Abbott et al. (DES), Phys. Rev. **D98**, 043526 (2018), 1708.01530.
- [39] M. R. Blanton et al. (SDSS), Astron. J. **154**, 28 (2017), 1703.00052.
- [40] N. Benitez et al. (J-PAS) (2014), 1403.5237.
- [41] A. Aghamousa et al. (DESI) (2016), 1611.00036.
- [42] C. L. Carilli and S. Rawlings, New Astron. Rev. **48**, 979 (2004), astro-ph/0409274.
- [43] C. M. Trott and J. C. Pober (2019), 1909.12491.
- [44] R. Bellman and K. M. R. Collection, *Adaptive Control Processes: A Guided Tour*, Princeton Legacy Library (Princeton University Press, 1961), URL <https://books.google.es/books?id=POAmAAAAAAAJ>.
- [45] E. A. Huerta et al., Nature Rev. Phys. **1**, 600 (2019), 1911.11779.
- [46] P. Mehta and D. J. Schwab, arXiv preprint arXiv:1410.3831 (2014).
- [47] R. Arjona and S. Nesseris (2019), 1910.01529.
- [48] S. Nesseris and A. Shafieloo, Mon. Not. Roy. Astron. Soc. **408**, 1879 (2010), 1004.0960.
- [49] S. Nesseris, D. Sapone, and J. Garca-Bellido, Phys. Rev. **D91**, 023004 (2015), 1410.0338.
- [50] D. Sapone, E. Majerotto, and S. Nesseris, Phys. Rev. **D90**, 023012 (2014), 1402.2236.
- [51] V. Rajpaul, in *Proceedings, 56th Annual Conference of the South African Institute of Physics (SAIP 2011): Gauteng, South Africa, July 12-15, 2011* (2012), pp. 519–524, 1202.1643.
- [52] A. Montiel, R. Lazkoz, I. Sendra, C. Escamilla-Rivera, and V. Salzano, Phys. Rev. **D89**, 043007 (2014), 1401.4188.
- [53] S. Yahya, M. Seikel, C. Clarkson, R. Maartens, and M. Smith, Phys. Rev. **D89**, 023503 (2014), 1308.4099.
- [54] S. Nesseris and D. Sapone, Int. J. Mod. Phys. **D24**, 1550045 (2015), 1409.3697.
- [55] C. Bogdanos and S. Nesseris, JCAP **0905**, 006 (2009), 0903.2805.
- [56] S. Nesseris and J. Garcia-Bellido, JCAP **1211**, 033 (2012), 1205.0364.
- [57] A. Shafieloo, A. G. Kim, and E. V. Linder, Phys. Rev. **D85**, 123530 (2012), 1204.2272.
- [58] S. Nesseris, G. Pantazis, and L. Perivolaropoulos, Phys. Rev. **D96**, 023542 (2017), 1703.10538.
- [59] S. Nesseris and J. Garca-Bellido, Phys. Rev. **D88**, 063521 (2013), 1306.4885.
- [60] A. Moradinezhad Dizgah and R. Durrer, JCAP **1609**, 035 (2016), 1604.08914.
- [61] B. Ghosh and R. Durrer, JCAP **1906**, 010 (2019), 1812.09546.
- [62] F. Skara and L. Perivolaropoulos (2019), 1911.10609.
- [63] R. Jimenez and A. Loeb, Astrophys. J. **573**, 37 (2002), astro-ph/0106145.
- [64] E. Gaztanaga, A. Cabre, and L. Hui, Mon. Not. Roy. Astron. Soc. **399**, 1663 (2009), 0807.3551.
- [65] H. Yu, B. Ratra, and F.-Y. Wang, Astrophys. J. **856**, 3 (2018), 1711.03437.
- [66] D. M. Scolnic et al., Astrophys. J. **859**, 101 (2018), 1710.00845.
- [67] A. Conley et al. (SNLS), Astrophys. J. Suppl. **192**, 1 (2011), 1104.1443.
- [68] F. Beutler, C. Blake, M. Colless, D. H. Jones, L. Staveley-Smith, L. Campbell, Q. Parker, W. Saunders, and F. Watson, Mon. Not. Roy. Astron. Soc. **416**, 3017 (2011), 1106.3366.
- [69] L. Anderson et al. (BOSS), Mon. Not. Roy. Astron. Soc. **441**, 24 (2014), 1312.4877.
- [70] X. Xu, N. Padmanabhan, D. J. Eisenstein, K. T. Mehta, and A. J. Cuesta, Mon. Not. Roy. Astron. Soc. **427**, 2146 (2012), 1202.0091.
- [71] C. Blake et al., Mon. Not. Roy. Astron. Soc. **425**, 405 (2012), 1204.3674.
- [72] A. J. Ross, L. Samushia, C. Howlett, W. J. Percival, A. Burden, and M. Manera, Mon. Not. Roy. Astron. Soc. **449**, 835 (2015), 1409.3242.
- [73] H. Gil-Marín et al., Mon. Not. Roy. Astron. Soc. **460**, 4210 (2016), 1509.06373.
- [74] T. M. C. Abbott et al. (DES), Mon. Not. Roy. Astron. Soc. **483**, 4866 (2019), 1712.06209.
- [75] M. Blomqvist et al., Astron. Astrophys. **629**, A86 (2019), 1904.03430.
- [76] J. E. Bautista et al., Astrophys. J. **863**, 110 (2018), 1712.08064.
- [77] M. Ata et al., Mon. Not. Roy. Astron. Soc. **473**, 4773 (2018), 1705.06373.
- [78] D. J. Eisenstein and W. Hu, Astrophys. J. **496**, 605 (1998), astro-ph/9709112.
- [79] B. Sagredo, S. Nesseris, and D. Sapone, Phys. Rev. **D98**, 083543 (2018), 1806.10822.
- [80] W. J. Percival and M. White, Mon. Not. Roy. Astron. Soc. **393**, 297 (2009), 0808.0003.
- [81] Y.-S. Song and W. J. Percival, JCAP **0910**, 004 (2009), 0807.0810.
- [82] S. Nesseris and L. Perivolaropoulos, JCAP **0701**, 018 (2007), astro-ph/0610092.
- [83] L. Kazantzidis and L. Perivolaropoulos, Phys. Rev. **D97**, 103503 (2018), 1803.01337.
- [84] S. Nesseris and S. Tsujikawa, Phys. Rev. **D90**, 024070 (2014), 1402.4613.
- [85] P. Zhang, M. Liguori, R. Bean, and S. Dodelson, Phys. Rev. Lett. **99**, 141302 (2007), 0704.1932.
- [86] R. Reyes, R. Mandelbaum, U. Seljak, T. Baldauf, J. E. Gunn, L. Lombriser, and R. E. Smith, Nature **464**, 256 (2010), 1003.2185.
- [87] A. M. Pinho, S. Casas, and L. Amendola, JCAP **1811**, 027 (2018), 1805.00027.
- [88] C. Bogdanos and S. Nesseris, AIP Conf. Proc. **1241**, 200 (2010).
- [89] S. Weinberg, *Cosmology* (2008), ISBN 9780198526827, URL <http://www.oup.com/uk/catalogue/?ci=9780198526827>.
- [90] L.-M. Wang and P. J. Steinhardt, Astrophys. J. **508**, 483 (1998), astro-ph/9804015.
- [91] S. Nesseris, C. Blake, T. Davis, and D. Parkinson, JCAP

1107, 037 (2011), 1107.3659.